Visual mental imagery in typical imagers and in aphantasia: A millimeter-scale 7-T fMRI study

Jianghao Liu[1,2*], Minye Zhan[3], Dounia Hajhajate[1], Alfredo Spagna[4], Stanislas Dehaene[3,5], Laurent Cohen[1,6], Paolo Bartolomeo[1]

[1]Sorbonne Université, Inserm, CNRS, Paris Brain Institute, ICM, Hôpital de la Pitié-Salpêtrière, 75013 Paris, France

[2]Dassault Systèmes, Vélizy-Villacoublay, France

[3]Cognitive Neuroimaging Unit, Université Paris-Saclay,CEA, INSERM, CNRS ELR9003, NeuroSpin center, 91191 Gif/Yvette, France

[4]Department of Psychology, Columbia University in the City of New York, NY, 10027, USA

[5]Collège de France, Université Paris-Sciences-Lettres (PSL), 11 Place Marcelin Berthelot, 75005 Paris, France

[6]AP-HP, Hôpital de la Pitié Salpêtrière, Fédération de Neurologie, Paris, France

*Correspondence: jianghao.liu@icm-institute.org

Abstract

Most of us effortlessly describe visual objects, whether seen or remembered. Yet, around 4% of people report congenital aphantasia: they struggle to visualize objects despite being able to describe their visual appearance. What neural mechanisms create this disparity between subjective experience and objective performance? Aphantasia can provide novel insights into conscious processing and awareness. We used ultra-high field 7T fMRI to establish the neural circuits involved in visual mental imagery and perception, and to elucidate the neural mechanisms associated with the processing of internally generated visual information in the absence of imagery experience in congenital aphantasia. Ten typical imagers and 10 aphantasic individuals performed imagery and perceptual tasks in five domains: object shape, object color, written words, faces, and spatial relationships. In typical imagers, imagery tasks activated left-hemisphere fronto-parietal areas, the relevant domain-preferring areas in the ventral temporal cortex partly overlapping with the perceptual domain-preferring areas, and a domain-general area in the left fusiform gyrus (the Fusiform Imagery Node). In aphantasic individuals, imagery activated similar areas, but the Fusiform Imagery Node was functionally disconnected from fronto-parietal areas. Our results unveil the domain-general and domain-specific circuits of visual mental imagery, their functional disorganization in aphantasia, and support the general hypothesis that conscious visual experience - whether perceived or imagined - depends on the integrated activity of high-level visual cortex and fronto-parietal networks.

Introduction

Visual mental imagery is the ability to experience visual information in the absence of actual external stimuli. However, approximately 4% of individuals report experiencing weak or absent visual mental imagery (Dance et al., 2022), a condition known as congenital aphantasia (Zeman et al., 2015). Surprisingly, individuals with congenital aphantasia can typically provide accurate answers from memory to questions on the visual appearance of objects, despite the absence of subjective imagery experience. For example, these individuals can correctly indicate which fruit is darker red between strawberries or cherries (Liu & Bartolomeo, 2023). What are the neural mechanisms responsible for accurate information processing in the absence of experiential correlates? Aphantasia provides a unique window into the mechanisms underlying conscious processing and awareness.

Rival models of visual mental imagery either claim that it depends on top-down signals from prefrontal regions to early visual areas (EVA) (Kosslyn et al., 1995; Pearson, 2019), or that it involves coordinated activity between frontoparietal (FP) networks and high-level visual regions in the ventral temporal cortex (VTC) (Spagna et al., 2021). These models make different predictions on the neural bases of inter-individual differences in subjective imagery vividness, which would either depend on the level of EVA activation (Pearson et al., 2015), or on different patterns of activity in VTC/FP circuits.

So far, neuroimaging has not been able to adjudicate between those two options, due to i) the difficulty to demonstrate a causal link between activations (e.g. in EVA) and imagery processes, and ii) the limited spatial resolution and group averaging which did not allow to dissociate closely packed visual regions with potentially distinct contributions to imagery and perception, e.g. group-averaging BOLD response in aphantasia (Milton et al., 2021). Evidence from acquired brain lesions (Bartolomeo et al., 1998, 2020; Behrmann et al., 1992; Spagna, 2022), which show preserved imagery in patients with lesions to the EVA or their connections strongly suggest that EVA is not necessary for visual mental imagery. Instead, lesion studies revealed impaired imagery after extensive damage to the left temporal lobe

(Bartolomeo et al., 2002; Liu et al., 2022; Moro et al., 2008). These studies also showed the possibility of selective imagery deficits for specific visual domains, such as object shape, object color, written words, faces, and spatial relationships (Bartolomeo et al., 2002; Goldenberg, 1993). This evidence suggests that domain-general and domain-specific mechanisms of visual mental imagery should be carefully distinguished. In comparison to some neuroimaging studies, lesion studies possess causal power (Bartolomeo et al., 2020), but are affected by issues like lesion-induced plastic reorganization and limited spatial resolution. Moreover, given the individual variability in the topographical organization of the VTC (Conway, 2018; Grill-Spector & Weiner, 2014), assessing the degree of overlap of activations between imagery and perception requires the use of methods with high spatial resolution in individual participants.

Here we circumvent those limitations by i) using ultra-high field 7-Tesla fMRI during tightly matched imagery and perceptual tasks in the five visual domains suggested by lesion studies: object shape, object color, written words, faces, and spatial relationships, ii) studying typical imagers but also, rather than patients with acquired lesions, individuals with aphantasia. This allowed us to: i) identify the neural circuits involved in voluntary visual mental imagery in individual participants; ii) compare them with those engaged in visual perception; iii) uncover the neural processes associated with diminished imagery experience in aphantasia. We predicted that, under the EVA hypothesis, typical imagers would exhibit normal activities including EVA activation, representational content and connectivity, whereas those with aphantasia would demonstrate dysfunctional EVA activity or connectivity. Under the VTC/FP hypothesis, by contrast, aphantasia should be associated with abnormal activity or connectivity in VTC/FP regions.

Results

Ten typical imagers (mean age = 29.28, SD = 8.47, 6 female) and 10 individuals with congenital aphantasia (mean age = 28.69, SD = 8.27, 6 female) performed our enhanced

Batterie Imagerie / Perception - eBIP (Liu & Bartolomeo, 2023) while undergoing 7T fMRI whole-brain scanning at 1.2 mm isotropic resolution (NeuroSpin, France). All participants were native French speakers. The eBIP comprises 162 trials, each one testing participants' performance on: (1) Mental imagery in response to auditory questions in five distinct domains (Fig. 1A-E): shapes, colors, written words, faces, and spatial relationships of cities on an imagined map of France; (2) a matched control task using abstract words to engage non-visual semantics while minimizing the involvement of visual imagery (Fig. 1F); (3) a perceptual task using the same items as the imagery tasks (Fig. 1G) but with the simultaneous presentation of auditory questions and the relevant pictorial items. Within the imagery and perceptual tasks, trials from the five domains were fully randomly presented. In the imagery task, participants rated the intensity of their visual imagery at the end of each trail using a 4-point Likert scale where a score of 4 indicated highly vivid imagery. In the abstract word task and the perception task, the rating of visual vividness was substituted with a confidence rating using a 4-point Likert scale, where a score of 4 represented absolute certainty. Accuracy and response time (RT) were recorded. We will first present the behavioral findings, then the fMRI findings for typical imagers by comparing imagery and perception, and finally the fMRI findings for aphantasic individuals.

Behavioral results

For typical imagers, the average trial-by-trial vividness score was 3.52 on a scale of 1 to 4, while for aphantasics individuals it was on average in 1.11 (Bayes Factor, BF = 5.387×10^{11}, see Fig. S1B for all behavioral results). Nevertheless, aphantasic individuals exhibited comparable levels of accuracy to typical imagers in both imagery (BF = 0.25) and perception (BF = 0.26). Their RTs were 0.21s slower on the imagery tasks and 0.43s slower on the perception tasks (BF = 30 and 85, respectively), and they had lower confidence in their responses on perceptual tasks (BF = 3.59), consistent with similar findings from a more extensive cohort of 117 participants (Liu & Bartolomeo, 2023). Importantly, however, there

was no evidence of group difference on either accuracy (BF = 0.46), RTs (BF = 0.41) or confidence scores (BF = 1.63) in the abstract words task, suggesting that the group difference was specific to visual items.

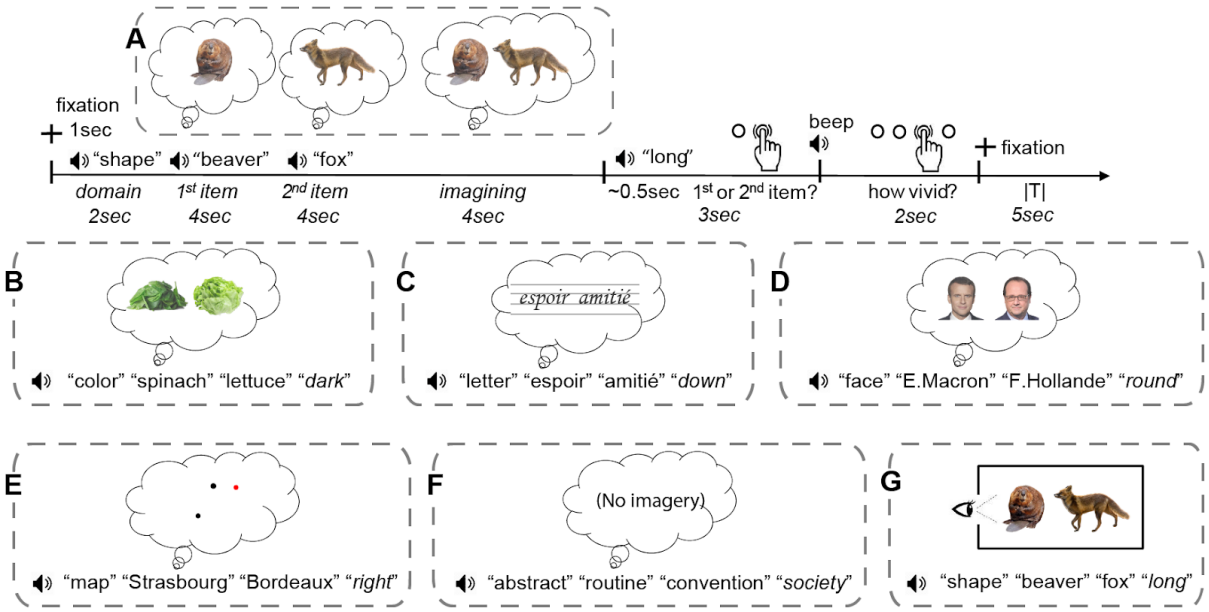

Fig 1. Tasks.
Examples of trials of the eBIP. The eBIP comprises imagery tasks of five domains: shapes, colors, letters, faces, and spatial relationships (A-E), a control task with abstract words (F), and a perception task (G) in five audio-visual domains using the same items as in the imagery tasks.

Domain-general and domain-specific activations, and V1 activity

Domain-general activations in typical imagers. We then combined all imagery domains to identify domain-general regions in typical imagers. The contrast of all averaged Imagery domains minus the abstract word task revealed a left-predominant set of regions (see Fig. 2A and Table S1) including the bilateral inferior frontal gyrus (IFG) and dorsal premotor cortex (PMd), the left intraparietal sulcus (IPS), and a region in the left posterior occipitotemporal sulcus (OTS; Talarach coordinates: -41, -55, -10), at coordinates almost identical to the FIN identified in our previous meta-analysis of fMRI studies (-40, -55, -11; Spagna et al., 2021). The comparison of all Imagery minus all Perception tasks did not show

any significant activation. The opposite contrast showed greater activation during perception than imagery in the bilateral lateral geniculate nucleus (LGN) and posterior occipitotemporal cortex (Fig. S2B, Table S1). Finally, Imagery tasks induced deactivations relative to baseline (Fig. S2C) in the bilateral medial prefrontal cortex (mPFC), posterior cingulate cortex (PCC), and left angular gyrus (ANG), which are known to be important nodes of the default mode network (Raichle, 2015), suggesting that participants were actively engaged during the imagery task.

Domain-specific activations in typical imagers. In both imagery and perception, we localized domain-preferring regions by contrasting activity elicited by each domain minus that of the other four domains. Importantly, however, there was substantial variability between individuals in the location of activations and each domain could activate multiple VTC neural patches. For example, the location of face-preferring fusiform patches showed substantial interindividual variability in perception (Fig. S3B), indicating limited efficacy of standard whole-brain group analysis methods. Thus, we report individual domain-preferring maps with a summary of regions that were consistently activated in at least 6 of the 10 typical imagers, and group-level results which show interindividual consistency of location, if any.

During imagery, (i) shape imagery activated the FG and superior occipital cortex; (ii) color imagery activated medial FG, PHG, posterior OTS, OFC, lFS, lPS; (iii) word imagery activated bilateral posterior OTS, lateral occipitotemporal cortex, dorsolateral prefrontal cortex (PFC) and lPS; (iv) face imagery activated OTS, mSTG, vPCC, vmPFC and OFC (adjacent and more lateral to the color imagery OFC areas); (v) map imagery activated PHG, lateral occipitotemporal cortex, posterior parietal area, precuneus, vPCC and dlPFC. Fig. 2B displays the results for a representative typical imager; see Figure S4 for all the others and Figure S3A and Table S1 for group-level maps.

On perception tasks, in line with previous research, (i) shape perception activated the left lateral occipital complex (LOC) and the bilateral medial fusiform gyrus (FG) (Kourtzi &

Kanwisher, 2001); (ii) color perception activated three patches in the bilateral medial FG, as well as the parahippocampal gyrus (PHG) (Lafer-Sousa et al., 2016) and the ventral orbitofrontal cortex (OFC); (iii) word perception activated the bilateral posterior FG, and bilateral FP regions (Gaillard et al., 2006); (iv) face perception activated the right OTS (FFA) and bilateral amygdala (Kanwisher et al., 1997); (v) maps of France activated the parahippocampal gyrus (PPA), the bilateral ventral posterior cingulate cortex (vPCC), precuneus, and angular gyri (Epstein et al., 1999). Fig. 2H displays these results for a representative typical imager; see and Fig. S3A and Table S2 for group-level maps.

In aphantasia. We then conducted the same activation analyses in aphantasic individuals. The contrast between Imagery and Abstract words tasks showed domain-general activations for imagery in the left IFG-IPS network, right dorsal FP areas, and, importantly, also in the FIN (Fig. 2C and Table S5, $p<0.001$, cluster-level size corrected). Importantly, during both imagery and perception, individuals with aphantasia demonstrated clear activation patterns in VTC domain-specific regions (all individual maps had $p<0.001$, without any data smoothing, and cluster size > 12 voxels; see Table S6 for perceptual domains; Fig. 2D for a representative aphantasic participant and detailed report of regions, and Fig. S5C for all the others for imagery domains; also see Table S5 for group-level results).

To test whether aphantasia had comparable activation level than typical imagers, we compared the FIN activation profile, and the number of activated voxels of domain-preferring areas between the two groups. There was no evidence for group differences in the FIN activation profiles (Bayesian repeated measure ANOVA with the factors of Group x Tasks, BF = 0.36). There was moderate evidence supporting similar activation patterns in aphantasic individuals as in typical imagers in all domains (3-way Bayesian ANOVA with the factor of Group x Region (EVA, ventral and dorsal visual pathways) x Domain. Main Group effect, BF = 0.21, see Fig.S5D).

V1 activity. If EVA plays a crucial role in mental imagery experience, then aphantasia

might be associated with abnormal EVA activity patterns. We compared the foveal V1 and the peripheral V1 activity between the two groups using Bayesian repeated measures ANOVAs (group x task). As expected, the foveal V1 manifested activation for the perceptual tasks without group differences (BF = 0.53, Fig. 2E). However, we observed negative activities in foveal V1 for the imagery tasks and for the abstract word task in both groups. Importantly, these negative activities in foveal V1 had lower activity amplitudes in aphantasia individuals than typical imagers during the imagery tasks (BF = 7.41), and also the abstract word task (BF = 3.47). No difference was found for peripheral stimuli (BF = 0.27) across the tasks between the two groups.

The FIN and domain-preferring activations. Unlike domain-preferring regions, FIN consisted in a single patch in all individual participants (Figure S6). Its location was partly overlapping with, but distinct from that of the VWFA. The FIN location was more mesial, rostral and ventral than that of the visual word form area (VWFA; Bayesian t-tests on coordinates, two-sided: x, BF = 2.57, y, BF = 3.20, z, BF = 6.59, see Figure S4 for individual maps). To assess the domain-general activity of the FIN, we conducted analyses using (i) conjunction of the activation maps of five single imagery domains versus baseline, and (ii) comparison of activation profiles between the FIN and the VWFA (Fig. 2F). Results confirmed that the FIN is a functionally unique region involved in domain-general imagery, with a partly overlapping yet separate localization from the VWFA in the lateral OTS in both typical imagers and aphantasic individuals (see Fig. S5A, Fig. S6 and S7 for details).

Overlap between imagery- and perception-induced activity. Importantly, by comparing unsmoothed individual patches, for all five domains, imagery-related activations overlapped with some of the perceptual-related activations in high-level VTC visual areas, FP and subcortical regions (e.g. amygdala for faces), but it was not observed in EVA despite stimulus-dependent EVA activation during perception (Fig. 2G). For example, color perception evoked activation in three color patches located bilaterally along the medial FG,

from posterior to anterior, as previously described by Lafer-Sousa et al. (2016). However, during color imagery tasks, only the anterior color patch was activated (-29, -35, -13; for 6 typical imagers out of 10 in the left hemisphere, for one in the right, for 2 bilaterally), whereas the posterior color patch did not show any significant activation (see Fig. 2H).

In summary, typical imagers and individuals with aphantasia displayed similar imagery-related activation in FP networks, in a domain-general region in the left FG, and in the relevant domain-preferring areas, with some overlapping with perception-related activity in more rostral patches.

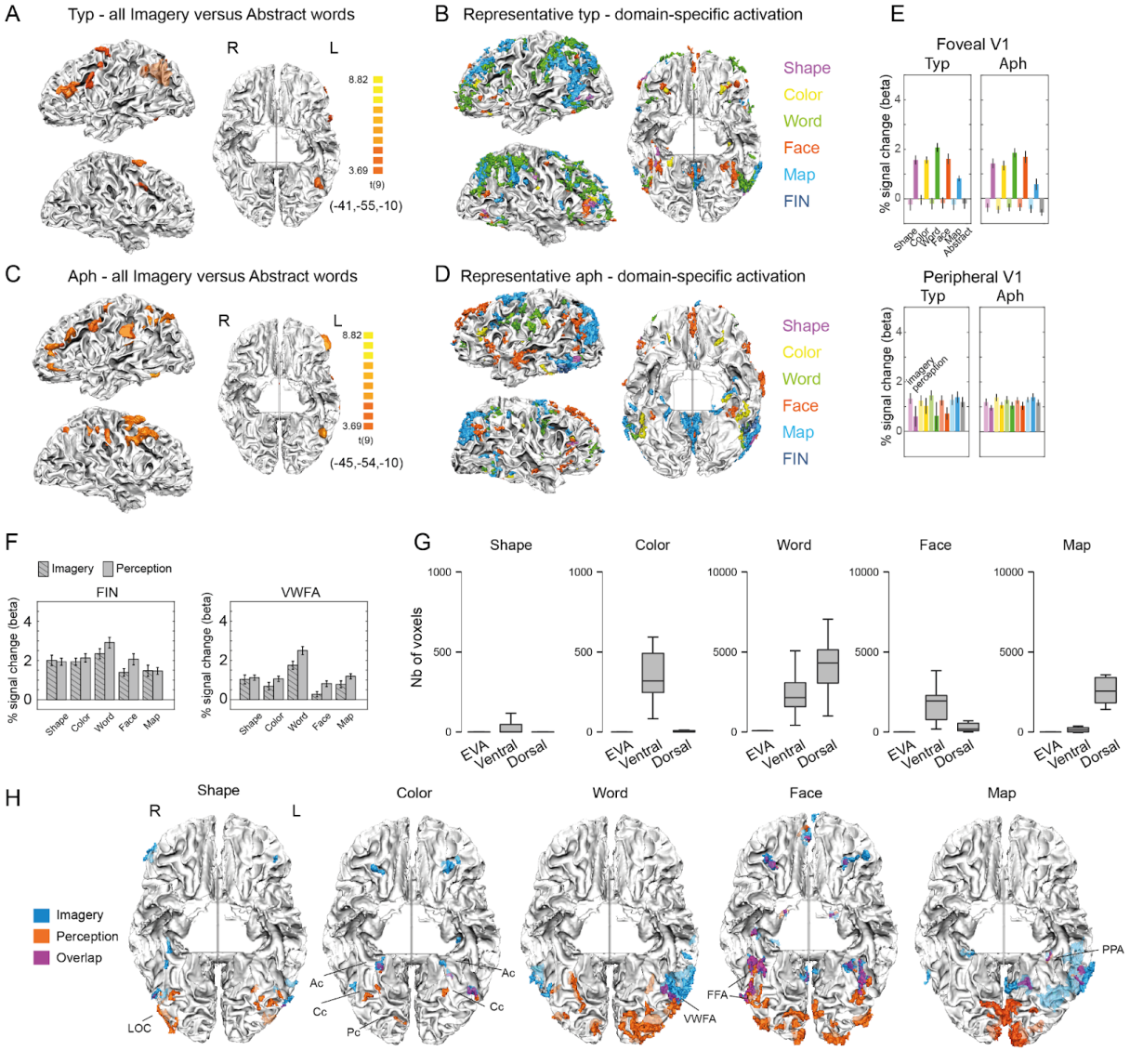

Fig 2. Patterns of BOLD response during imagery, and their overlap with perception in typical imagers and aphantasic individuals.

(A) Group-level contrast of all Imagery minus Abstract words in typical imagers. Orange-colored patches indicate higher activation in imagery tasks than in the Abstract words task. Note that domain-general regions are mostly left-lateralized. All group-level maps underwent cluster-size thresholding using Monte-Carlo simulation with an alpha level of 0.05 and 5,000 simulations, and an initial threshold of $p<0.005$. The functional data was smoothed with a full width at half maximum of 6 mm.

(B) Domain-specific activation during single imagery domains in a representative typical imager (Typ 05), from the contrast of one domain > the other 4 domains. All individual-level maps were thresholded at $p<0.001$, without any data smoothing, and cluster size > 12 voxels. The different domains and the FIN are color-coded.

(C) Group-level contrast of all Imagery minus Abstract words in aphantasic individuals. $p<0.001$, cluster-level size corrected.

(D) Domain-specific activation during single imagery domains in a representative aphantasic individual (Aph10). (i) shape imagery activated the lateral FG; (ii) color imagery activated the left medial FG, IFS and bilateral PHG, OFC; (iii) word imagery activated bilateral lateral FG, OTS and bilateral IPS and right MFG, PMd; (iv) face imagery activated bilateral OTS, STG, amygdala, OFC, medial PFC, vPCC; (v) map imagery activated bilateral PHG, left LOC and bilateral ANG, Precuneus, PMd, vPCC.

(E) Group-level activity profile of signal change in the peripheral V1 and the foveal V1. Typ: typical imagers; Aph: aphantasic individuals. Error bars represent +/– 1 normalized SE across participants. Lighter colors indicate activation for imagery domains and darker colors indicate perceptual domains. Note the negative activity in foveal V1 for the imagery tasks and for the abstract word task.

(F) Group-level histogram of signal change in the FIN and the VWFA during imagery and perception for each domain. The VWFA was defined by contrasting the perception of Words minus the perception of other categories. Error bars represent +/- 1 normalized SE across participants.

(G) Box-and-whisker plots of the number of voxels showing domain-specific activation during both mental imagery and perception, in EVA (V1, V2, and V3), the ventral visual pathway, and the dorsal visual pathway. Voxels are unsmoothed individual domain-preferring patches. Such voxels were present only in high-level visual areas, but not in EVA. Boxplot shows values of median, upper quartile, lower quartile, maximum and minimum, respectively.

(H) Domain-specific activations during perception (orange), during imagery (blue), and their overlap (purple), in a representative typical imager (Typ 05). Only the ventral view is displayed. Pc, Cc and Ac indicate the posterior, central, and anterior color-biased regions, respectively.

Representational content of imagery activations

We used representational dissimilarity matrices (RDMs) (Kriegeskorte, 2008) to assess the type of information processed by the imagery-activated regions and by V1 from the all

Imagery *minus* the abstract word contrast (Table S1, Table S5). To determine whether the different regions coded stimuli according to domain, and whether codes were similar across perception and imagery, we computed multivoxel pairwise correlation between the spatial patterns of BOLD response elicited by the 90 imagery items and by the 30 perceptual items, thereby revealing their representation in a higher-order space.

For perception tasks (Fig. 3A and Fig. S8, darker blue areas), the RDMs featured small blocks around the diagonal in V1, FIN, and left IPS regions. The RDMs in these regions were significantly correlated with a theoretical diagonal domain matrix, suggesting the presence of domain-content information in all these regions (all Bayesian correlation values of Pearson rs > 0.27; BFs > 1.19e6; n = 435), and showed highly similar representation between groups in V1 (r = 0.61, n = 435, BF = 1.08e42); this was also true for the FIN (r = 0.24, BF = 1.44e5), but not for FP regions (all rs<0.15; BFs < 8.81).

For imagery tasks, there were similar diagonal domain blocks patterns in the RDMs for FIN, left IPS, and IFG (Fig. 3B, all Bayesian correlation values with theoretical matrix rs > 0.14; BFs > 1.61e14; n = 4005). RDMs showed high similarity between typical imagers and aphantasic individuals (Fig.6B, r = 0.09; BF = 2.32e5 for the FIN; r = 0.13, BF = 1.11e14 for the left IPS; r = 0.09, BF = 1.11e6 for the IFG; Talarach coordinates: -41, 31, 17). However, for imagery there was no evidence of RDM diagonal domain blocks for V1 (r<0.04, BF<1.09), and no comparable representations between groups (r = 0.05, BF = 3.24).

We further assessed within-group variability by calculating the correlation between each participant's RDM and the mean RDM derived from the remaining individuals within the same group. For either group, there was no evidence of any differences in within-group consistency of these regions (all BFs < 2.51).

Correlations between imagery and perceptual RDMs, where participants imagined or perceived the same items, were higher in the FIN for typical imagers than for aphantasic individuals (Bayesian t-test, BF = 8.15, Fig. S8B); unexpectedly, correlations were instead higher for aphantasic individuals than for typical imagers in the left PMd (Talarach

coordinates: -34, -2, 57; BF = 5.83). Critically, the strength of imagery-perception similarity of the FIN in typical imagers was strongly correlated with individual vividness VVIQ scores (r = 0.82, BF = 14.04, Fig. S8C). However, in V1, there was moderate evidence to reject the correlation of imagery-perceptual representations (BF = 0.24, Fig S10D) and no support for group difference (BF = 0.41).

In summary, typical imagers and aphantasic individuals showed differences in perceptual/imagery correlations in FIN and premotor cortex, but similar imagery representations in FIN and FP regions, and similar perceptual representations in FIN and V1.

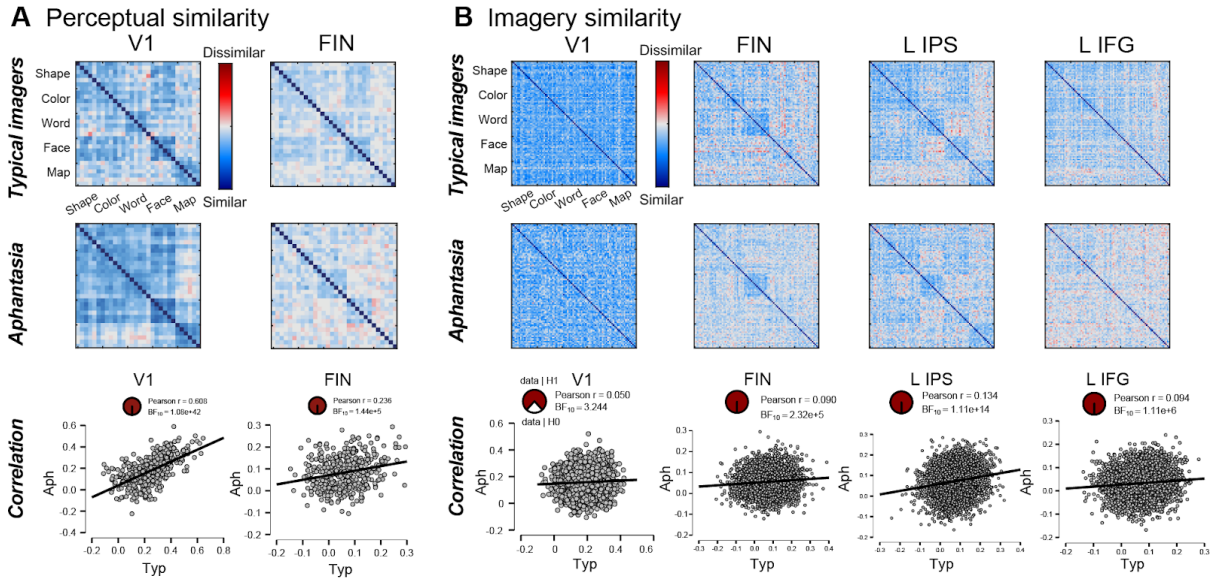

Fig 3. Representational similarity between typical imagers and aphantasics

(A) Group-averaged representational dissimilarity matrix and between-group correlation of perceptual RSM for 30 different items. The emergence of small diagonal domain blocks, indicated by the darker blue areas, shows a similarity that is specific to that domain. Typ, typical imagers; Aph, aphantasic individuals. Each dot in the scatter plot represents a cell value in the RSM, indicating the pairwise correlation between two items, in the respective groups along the two axes. The correlation coefficient is thus a measure of the resemblance between the mean RSMs of Typ and Aph groups.

(B) Group-averaged representational dissimilarity matrix and between-group correlation of imagery RSM for 90 different items. Typ, typical imagers; Aph, aphantasic individuals.

Task-modulated and task-residual functional connectivity

How do activity patterns in these cortical regions change in relation to one another and in relation to the behavioral tasks? We used psychophysiological interaction (PPI) analysis to examine task-specific functional connectivity between the V1 / FIN and other brain regions.

FIN connectivity in typical imagers. To explore domain-general connectivity, we looked for regions whose correlation with the FIN would be higher during all Imagery than during the Abstract words task, which revealed bilateral OFC regions (Fig. S9A). We then compared the connectivity of the FIN between the “all Imagery” and the “all Perception” conditions. During imagery, we observed higher connectivity with the left OFC, mSTS and the right anterior temporal lobe (ATL). During perception, we found higher FIN connectivity with bilateral posterior occipitotemporal visual areas. To examine domain-specific connectivity, we compared each perceptual or imagery domain minus Abstract words using PPI analysis. We observed increased FIN connectivity with dorsolateral FP areas, domain-preferring VTC regions and subcortical areas in both imagery and perceptual domains (Imagery: Table S3, see Fig. 4A for colors and faces, Fig. S9B for the other domains; Perception: Table S4, see Fig. 4B for colors and faces, Fig. S9B for the other domains).

FIN connectivity in aphantasia. Despite similar local BOLD responses, there was a sharp difference between aphantasic individuals and typical imagers in the functional connectivity of the FIN. In aphantasic individuals, no brain region displayed increased functional connectivity with the FIN in either the contrast of all Imagery vs. Abstract words or the contrast of all Imagery vs. all Perception. When contrasting all Perception to Abstract words in aphantasic individuals, the FIN exhibited greater connectivity during Perception with bilateral occipitotemporal regions and the right-hemisphere IFG and SMG, which are components of the brain reorienting network (Corbetta et al., 2008; Liu et al., 2023). In contrast, when comparing single imagery or perceptual domains with Abstract words, we did not observe any measurable functional connectivity between the FIN and dorsal FP regions in aphantasic individuals during either imagery or perception. Specifically, concerning imagery domains, in aphantasic individuals the FIN displayed higher local connections with FG in color imagery and right vPCC in map imagery (Fig. 4C, Table S7). No significant connectivity was found for the imagery of shapes, faces, and maps. In perceptual domains, the FIN

349 showed only local higher connectivity with areas in the occipitotemporal region for the
350 perception of shapes, colors, words, and faces (Fig. 4D and Table S7). Word perception
351 induced also a higher FIN connection with right anterior PFC. No significant connectivity was
352 observed in the perception of maps. Importantly, this absence of measurable functional
353 connectivity pattern is consistent across all aphantasic individuals.

354 Directly comparing patterns of FIN connectivity between the two groups revealed that
355 typical imagers displayed stronger connectivity during domain-general imagery than for either
356 Abstract words or Perception with the left anterior PFC, OFC, and MTG/STG compared to
357 aphantasic individuals (Fig. 4E). Regarding domain-specific connectivity, Fig. 4F and Fig.
358 S10 displays FIN connectivity differences between typical imagers and aphantasic individuals
359 for each imagery and perceptual domain.

360 **V1 connectivity.** Comparing all Imagery versus Abstract words, in typical imagers,
361 the foveal V1 showed higher connectivity with bilateral calcarine sulcus and left middle
362 temporal gyrus. The peripheral V1 had higher connectivity with left precuneus and posterior
363 middle frontal gyrus. In aphantasia, the foveal V1 had higher connectivity with bilateral
364 calcarine sulcus, medial PFC, precuneus, temporoparietal junction. The peripheral V1
365 displayed higher connectivity with bilateral lateral FG. There were no significant group
366 differences in either foveal or peripheral V1 connectivity.

367 **Task-residual connectivity.** Next, we regressed out the task-related activity (see
368 Methods) to obtain task residual data in imagery runs, and derive a proxy for resting-state
369 functional connectivity. Using the FIN as seed, we observed connectivity with the bilateral
370 supplementary motor area, precuneus, V1, left MFG, FG and right IPS in typical imagers (Fig.
371 S9C) and with bilateral V1 and right MFG in aphantasic individuals. No significant group
372 difference was observed in task-residual connectivity.

373 In summary, in typical imagers the FIN is functionally connected with FP areas and
374 with the relevant domain-preferring regions in domain-specific tasks, during both imagery and

perception. Aphantasic individuals showed no measurable functional connectivity between the FIN and other regions in either imagery or perception.

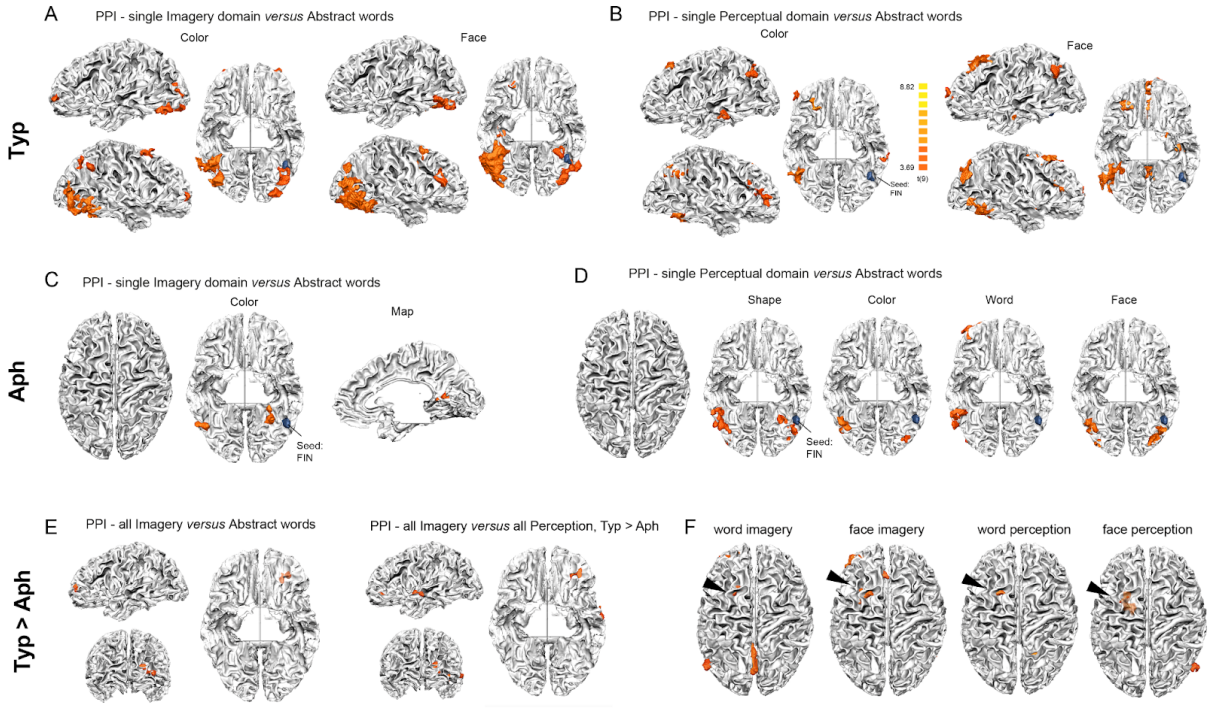

Fig 4. Group-level task-specific functional connectivity of the FIN during imagery and perceptual domains in typical imagers and in aphantasia individuals.

(A) PPI for single Imagery domain minus Abstract words in typical imagers. The seed was individual FIN. Examples in color and face domains. The FIN was connected with: bilateral ANG, left MTG, SFG, right FG, SMG, IFG and OFC, for color imagery; bilateral amygdala, PMd, left MTG, PHG, vPCC, IPS and right FG, ANG, dmPFC, OFC, for face imagery.

(B) PPI for single Perceptual domain minus Abstract words in typical imagers.

(C) PPI for single Imagery domain minus Abstract words in aphantasic individuals. Note that no FP region was significantly more connected with the FIN and no region was significantly more connected in the shape, word, and face imagery domains than during the Abstract words task.

(D) PPI for single Perceptual domain minus Abstract words in aphantasic individuals. No FP region was significantly more connected with the FIN and no difference in connectivity was measurable during map perception.

(E) Group difference of imagery domain-general FIN connectivity. Orange shows regions with higher connectivity in typical imagers than in aphantasics.

(F) Examples of group differences of FIN connectivity by domains (PPI, single domain *versus* Abstract words). Black arrows indicate the left PMd region consistently more connected to the FIN in typical imagers than in aphantasic individuals during both imagery and perception.

Higher activation in aphantasia

Last, we compared brain activation between the two groups of participants by using whole-brain ANOVAs. During all Imagery minus baseline, aphantasic individuals showed higher activation than typical imagers in the right-hemisphere IFG, SMG, IPS, pMTG and a in a left occipital area (see Fig.5A and Table. S8). These same right-hemisphere FP regions were activated in aphantasic individuals but *deactivated* in typical imagers during all Imagery *versus* baseline. PPI analysis with IFG, SMG, IPS as seed revealed that these regions were more connected with *left*-hemisphere MTG, pSTG and right mSTG in Imagery *versus* Abstract words for aphantasic individuals (Fig. 5B and Table S9). Notably, during perception the same right-hemisphere IFG-SMG network exhibited higher activation in aphantasic individuals than in typical imagers (Fig. 5C) and connected to left MTG, IFG in Perception *versus* Abstract words for aphantasic individuals (Fig. 5D). Results from the control task with Abstract words showed no activation difference between groups.

Concerning domain-specific imagery activation, no areas other than the right hemisphere IFG-SMG domain-general network were differentially activated between groups, except during face perception, where typical imagers displayed greater activation in the left FG, medial to the FIN, compared to aphantasic individuals (Fig. S10A).

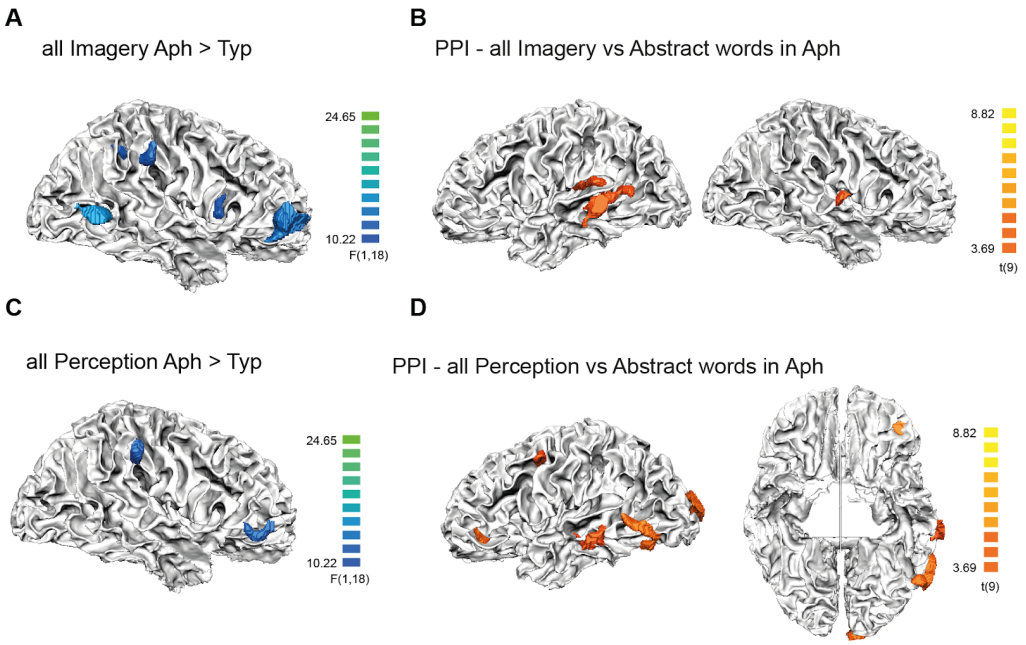

Fig 5. Higher activation in right-hemisphere regions in aphantasia

(A) Group difference in all Imagery domains minus baseline. Blue shows regions with higher activation in aphantasic individuals than in typical imagers. Typ: typical imagers. Aph: aphantasic individuals.

(B) PPI for the contrast of all Imagery domains vs Abstract word task in aphantasic individuals, with the FP regions found in the group difference on all Imagery activation (right IFG, SMG, IPS) as seed (see cluster size in Table S8).

(C) Group difference in all Perception domains minus baseline. Regions with higher activation in aphantasic individuals than in typical imagers are shown in blue.

(D) PPI for the contrast of all Perception domains vs Abstract word task in aphantasic individuals (see region details in Table.S9), with the FP regions found in the group difference on all Perception activation (right IFG, SMG) as seed.

Discussion

We used ultra-high-field fMRI to identify key cortical circuits of visual mental imagery in typical imagers and in individuals with congenital aphantasia, who claim not to experience any visual mental imagery during wakefulness. Our study involved comprehensive testing of visual mental imagery capabilities across five different domains, namely object shapes, object colors, faces, letters, and spatial relationships. Aphantasic individuals had comparable levels of accuracy to typical imagers but they responded more slowly in both imagery and perception tasks, confirming previous findings (Liu & Bartolomeo, 2023). They were also less confident than typical imagers in their responses on perceptual tasks, but not on the abstract word task, which suggests a vision-specific phenomenon (Morales et al., 2018). In typical imagers, imagery tasks activated (i) domain-preferring VTC and FP regions for each of the five explored imagery domains; (ii) a domain-general node around the posterior lateral OTS in the left hemisphere, a location consistent with the Fusiform Imagery Node (FIN) as identified in our recent meta-analysis (Spagna et al., 2021); (iii) left-lateralized domain-general IFG-IPS areas. We will now discuss the role of these cortical regions in imagery, their relative contribution to conscious imagery experience, and the neural signatures of its absence in aphantasia.

A domain-general imagery node in the left fusiform gyrus. The FIN was consistently active during visual mental imagery, independent of the imagery domain. Left temporal activity at locations close to the FIN was previously described during image generation and synthesis (D'Esposito et al., 1997; Yomogida et al., 2004), and to correlate with reported imageability during the solution of advanced mathematical problems (Amalric & Dehaene, 2016). The observation of functional connectivity between FIN and dlPFC / OFC dovetails nicely with the anatomical connectivity of the FIN to these regions (Hajhajate et al., 2022), and support its role as a domain-general node at the confluence of top-down

influences from the FP networks and horizontal connections with the VTC domain-preferring regions.

Anatomically, the FIN is contiguous to domain-preferring VTC regions such as VWFA or the FFA, such that one may ask whether it is topographically distinct from those regions. The present results localize the FIN around the left-hemispheric posterior OTS in 19 participants of 20. Specifically, individual analyses showed that the FIN, containing a single patch, tended to be more mesial, rostral and ventral than the VWFA. Its location was sandwiched between the VWFA laterally and FFA mesially, with a possible partial overlap with these regions.

Our findings substantiate the hypothesis that the FIN has a very specific involvement in both imagery and perception, based on the following functional attributes. First, the FIN showed domain-generality by its increased BOLD activation when performing imagery tasks in all five domains: object shape, object color, written words, faces, and spatial relationships. Second, the FIN, together with the left-hemisphere IFG/IPS (see Fig. 6A), coded semantic content in its multivoxel patterns of activity. Third, the FIN showed increased functional connectivity with FP networks and with the relevant domain-preferring regions during domain-specific tasks, consistent with a possible role for the FIN as a semantic control hub (Jackson, 2021) for task-relevant features in both imagery and perception. Moreover, the strong left lateralization of the FIN, as well as that of domain-general FP areas, is in line with abundant evidence on hemispheric asymmetries of voluntary generation of visual mental imagery (Farah, 1984; Liu et al., 2022). Such hemispheric asymmetry is also difficult to reconcile with the dominant model of visual mental imagery, which puts an emphasis on the implication of non-lateralized EVA. It is instead consistent with the predominant left-lateralization of the semantic system (Binder et al., 2009; Fernandino et al., 2022), which provides a main input to voluntary visual mental imagery. Thus, these results support the notion of a semantic contribution of the FIN to the construction of mental images.

Still, the stronger activation of the FIN during imagery tasks than during Abstract words processing might have an alternative explanation: the FIN could merely be a semantic region rostral to VWFA, specialized for concrete as opposed to abstract words. However, this possibility is unlikely, because the FIN appeared to be critically involved in mental imagery in studies using a variety of contrasts, some of which implemented non-verbal cues to evoke imagery (Spagna et al., 2021). The separation between domain-general and domain-specific functions in the VTC is likely to minimize the cost of long-distance wiring (Sporns & Betzel, 2016) thanks to locally dense connections between domain-preferring regions and the FIN, and sparser connections with more remote areas. The FIN, equipped with long-range connections with the perisylvian language network and the anterior temporal lobe, may thus act as a central hub for global back and forth communication between visual areas and language-related regions. Thus, the FIN may act as a bridge between semantic and visual information, enabling the generation of mental images with a visual content. This hypothesis also offers an explanation for the deficits in visual mental imagery observed in neurological patients, and yields testable predictions. Patients with lesions affecting the domain-general FIN, or disconnecting it from semantic networks, are likely to experience general imagery impairments (Bartolomeo, 2021; Moro et al., 2008). Lesions or disconnections that specifically target domain-preferring regions may result in more domain-specific patterns of mental imagery deficits (Bartolomeo et al., 2002). More posterior lesions disconnecting VTC from visual input are instead likely to produce perceptual deficits with preserved visual mental imagery (Bartolomeo, 2002, 2021).

The role of domain-preferring ventral temporal areas. Dissociations in performance across various imagery domains among neurological patients (Bartolomeo, 2002; Goldenberg, 1993) suggest the existence of domain-specific circuits for visual mental imagery of object shape, object color, written words, faces, and spatial relationships, which may partly overlap with the corresponding domain-preferring circuits in visual recognition (Bartolomeo et al., 2015; Conway, 2018; Dehaene & Cohen, 2011; Epstein et al., 1999;

Kanwisher et al., 1997; Kourtzi & Kanwisher, 2001; Lafer-Sousa et al., 2016; Mahon & Caramazza, 2011). Our findings clarify the topographical organization of VTC regions at an individual level using high-resolution functional imaging (see Fig. S4). Previous work showed FFA and PPA activity during imagery of faces and places, respectively (Ishai et al., 2000; O'Craven & Kanwisher, 2000). We replicated those findings in the FFA and PPA, and extended them by demonstrating imagery-related activity in the LOC for shape imagery, in the VWFA for letter imagery, and in color-biased regions for color imagery. Importantly, by comparing individual patches, we found that domain-preferring imagery activity specifically involves some of the domain-preferring perceptual regions in VTC in the high-level visual and associative areas, e.g. color imagery activates anterior color-biased patches but but not the posterior ones. In addition, we also found domain-preferring imagery activity in both dorsal FP networks, OFC and subcortical regions, such as in the amygdala for face imagery, possibly encoding associated emotions, and adjacent OFC patches for faces and colors.

The role of early visual areas in visual mental imagery. In both typical imagers and aphantasic participants, we observed peripheral V1 activation during imagery and perceptual tasks, as well as during the control task with abstract words. This activity might result from orienting of spatial attention in response to auditorily presented stimuli, which is often found in peripheral retinotopic locations of V1 (Brang et al., 2015; Cate et al., 2009). Importantly, however, foveal V1 was active in perception but showed negative activity in imagery and in the abstract words task. This can result from attention being endogenously directed toward internal thoughts, which may inhibit foveal V1 to prevent potential interferences from external input. These findings challenge standard models stressing the role of EVA in visual mental imagery (Kosslyn et al., 2001; Pearson, 2019). However the pattern we observed is quite consistent with extensive neuroimaging evidence in neurotypical individuals, which shows that visual mental imagery triggers activity in VTC and FP networks - but not in the EVA (Mechelli et al., 2004; Spagna et al., 2021). Moreover, detailed studies of neurological patients provided causal evidence through observations of disrupted imagery

following left temporal damage rather than following lesions restricted to the occipital cortex (Bartolomeo, 2002; Bartolomeo et al., 2020; Liu et al., 2022). In different experimental contexts, mental imagery of colors (Bergmann et al., 2019), or the expectation to see gratings (Aitken et al., 2020), have been shown to modulate activity in the deep layers of V1. However, the comparable V1 activity and connectivity of aphantasia in our study suggests that these V1 patterns have no causal contribution to conscious imagery experience, consistent with early suggestions (Crick & Koch, 1995).

The relationship between visual perception and visual mental imagery. Our findings elucidate three important aspects of typical visual mental imagery, indicating that imagery does share some neural substrates with visual perception (Dijkstra et al., 2019; Mechelli et al., 2004), but with prominent differences. First, domain-preferring VTC regions exhibited some overlap between imagery and perception in more rostral patches, whereas more caudal patches only responded to perception. Second, we identified distinct cortical patterns of representation for domain content between imagery and perception. Semantic domain information was encoded in FP regions, while the FIN exhibited top-down encoding, as opposed to the bottom-up encoding observed in V1 and FIN. This finding aligns with previously reported similarities in domain-specific visual areas between imagery and perception (Cichy et al., 2012; Reddy et al., 2010; Stokes et al., 2009). Third, the FIN displayed different functional connectivity patterns between imagery and perception. In imagery, it displayed stronger connections with semantic networks, whereas in perception, it showed greater connectivity with occipitotemporal areas. Taken together, this evidence emphasizes the importance of high-level visual cortex for imagery and the common role of the FIN in processing semantic and visual content for both imagery and perception.

Functional disconnection in aphantasia. Surprisingly, aphantasic individuals showed the engagement of similar brain networks during mental imagery as observed in typical imagers. This was confirmed by univariate and RSA analyses of BOLD responses, in

both domain-general and domain-preferring VTC areas, and in the FP networks. Consistent with this observation, aphantasic individuals were able to perform as accurately as typical imagers on tests of mental imagery (Liu & Bartolomeo, 2023). However, while typical imagers showed functional connection between the FIN with FP networks, aphantasic individuals did not display such correlations. Specifically, in aphantasics the FIN was functionally disconnected from the FP networks during both visual mental imagery and perception, which might explain their slower behavioral responses. In partial agreement with our results, Milton et al. (2021) compared resting-state functional connectivity between PFC and the visual–occipital network in aphantasic individuals and in individuals with particularly vivid visual mental imagery, and found reduced connectivity in aphantasia. Also in support of this idea, activity in a left-hemisphere mid-dorsolateral PFC area, close to the region we found in typical imagers, was associated with the processing of conscious stimuli relative to comparable but unconscious stimuli (Lau & Passingham, 2006). Reduced long-range connectivity is a hallmark of various neurodevelopmental disorders (Sokolowski & Levine, 2023). Within the framework of the Global Neuronal Workspace hypothesis of conscious perception (Dehaene et al., 2006; Mashour et al., 2020), such a functional disconnection between FIN and FP networks could be interpreted as depriving visual mental imagery of its conscious experiential content. In other words, VTC activity by itself might be sufficient to access visual information, but not to experience it as a conscious perception-like state. In line with our findings, the Global Neuronal Workspace hypothesis underscores the importance of long-range loops between different cortical areas in sustaining and broadcasting neural information across the brain, with the dorsolateral PFC cortex playing an essential role (Dehaene et al., 2006; Mashour et al., 2020). Hence, aphantasia, characterized as a relatively "pure" deficit in conscious imagery experience, with paradoxically preserved ability to perform imagery tasks, offers a compelling testing ground for theories of the brain mechanisms of conscious experience.

Increased activity in aphantasia. In both imagery and perception, the present group of aphantasic individuals exhibited greater activity in right-hemisphere IFG and SMG, which are important components of the right-lateralized network for reorienting attention (Bartolomeo & Seidel Malkinson, 2019; Corbetta et al., 2008) and its interaction with conscious perception (Liu et al., 2023). Such abnormal activity may play a role in disrupting the subjective experience of generating or maintaining mental imagery, for example by interrupting ongoing activity in more dorsal FP networks (Corbetta et al., 2008). A possible mechanism is defective filtering of distracting events (Shulman et al., 2007), leading to interference with internally generated models (Bartolomeo & Seidel Malkinson, 2022).

Limitations of the present study include: (1) The exclusion of bilateral anterior temporal lobes due to limited brain coverage at 7T (Fig. S2A). (2) The lack of parametric trial-by-trial vividness modulation in the analyses, which was not feasible in the group analysis because of insufficient variability in the vividness ratings of typical imagers (uniformly high) and of aphantasic individuals (uniformly low; Fig. S1C). (3) The possibility that aphantasia might be a heterogeneous condition, in the absence of diagnostic criteria that could identify potential subtypes with differing neural substrates.

Despite these limitations, our findings shed light on the left-predominant circuits of individual-level visual mental imagery, encompassing the FIN, FP networks, and domain-preferring VTC regions. This suggests the presence of distinct domain-general and domain-preferring cortical components. Our results also demonstrate that visual mental imagery and visual perception share similar neural mechanisms supporting high-level vision. Finally, we identified a neural signature of aphantasia, which was associated with a functional disconnection within the imagery network between the FIN and FP networks, despite essentially normal behavioral performance, BOLD activity levels, and representational content. Thus, the present results support the general hypothesis that conscious visual experience - whether perceived or imagined - depends on the integrated activity of FP

networks and high-level visual cortex (Dehaene et al., 2006; Liu et al., 2023; Mashour et al., 2020; van Vugt et al., 2018).

Acknowledgements

The research was supported by INSERM, CEA and specific funding from Dassault Systèmes. We are grateful to NeuroSpin support staff, and particularly to Bernadette Martins, the nurses and MR technicians at NeuroSpin who provided crucial help at various stages of data acquisition and analysis. The work of P.B. is supported by the Agence Nationale de la Recherche through ANR-16-CE37-0005 and ANR-10-IAIHU-06, and by the Fondation pour la Recherche sur les AVC through FR-AVC-017. J.L. expresses his gratitude for the 2023 European Workshop on Cognitive Neuropsychology Prize that was awarded to him in recognition of the work presented in this study.

Contributions

Conceptualization: J.L., P.B., L.C., S.D.; Data curation: J.L., D.H., M.Z.; Formal analysis: J.L., M.Z.; Investigation: J.L., D.H., M.Z.; Methodology: J.L., M.Z.; Funding acquisition: P.B., J.L.; Project administration: P.B.; Resources: S.D.; Software: J.L., M.Z.; Supervision: P.B.; Visualization: J.L.; Writing - original draft: J.L.; Writing - review & editing: All authors

Competing interest

The authors declare that they have no competing interests.

Materials & Correspondence

Requests for materials and correspondence should be addressed to J.L.

Method

1. Participants

Ten typical imagers (mean age ± SD, 29.28 ± 8.47, 6 female) were recruited from the CNRS RISC volunteer database (https://www.risc.cnrs.fr/). All typical imagers had average or high vivid mental imagery with VVIQ score greater than 55 (mean ± SD, 71.70 ± 7.07, out of a total score of 80). Ten individuals with congenital aphantasia (mean age ± SD, 28.69 ± 8.27, 6 female) were recruited from French-language groups on aphantasia in various online social media. All participants were right-handed. All aphantasic participants reported a *complete* life-long inability to generate visual mental imagery, and this was confirmed by an individual interview with author D.H. (a clinical psychologist) during the recruitment. All aphantasic individuals reported scored 16 out of 80 ("no image at all" for all questions) to the VVIQ. Interestingly, many aphantasics (8 out of 10) confirmed that they tend to perceive pictures with a *divide-and-label* strategy, akin to semantic conversion from visual features into content lists. While asked to visualize, they briefly recall the list of semantic labels to respond to the relevant question. Notably, they reported difficulties in remembering complex or unfamiliar pictures, which might reflect lower efficiency of the semantic encoding strategy in this case. All participants were right-handed with normal or corrected-to-normal vision and had no history of neurological/psychiatric disorders. Aphantasic participants did not differ from typical imagers in age ($t = 0.35$, $p = 0.73$, $d = 0.16$) or in education level ($t = 1.33$, $p = 0.20$, $d = 0.62$). Participants provided written consent before the study and received monetary compensation after the study. The study was approved by CEA and, according to French bioethical law, by a randomly selected regional ethical committee for biomedical research (CPP 100055 to NeuroSpin center) and the study was carried out in accordance with the declaration of Helsinki.

2. Introspective reports

Before the fMRI session, participants completed the French versions of the VVIQ (Santarpia et al., 2008) and OSIQ (Blajenkova et al., 2006) questionnaires to assess the subjective vividness of their visual mental imagery. The OSIQ consists of two scales assessing preferences for representing and processing of object imagery about pictorial and high-resolution images of individual objects, and of spatial imagery about semantic images and spatial relations amongst objects (see Supplementary materials for French translations). The results confirmed the drastic reduction of imagery ability in aphantasic individuals compared to typical imagers (VVIQ, BF = infinity; OSIQ object, BF = 2.06×10^{9}), but no reduction in spatial ability (OSIQ spatial: BF = 0.46).

3. Stimuli and fMRI experiment design

In the scanner, participants performed a longer version of the enhanced Battérie Imagerie-Perception - eBIP (Liu & Bartolomeo, 2023). The current version of the battery assesses (1) imagery of object shapes (Fig. 1A), object colors (Fig. 1B), faces (Fig. 1C), letters (Fig. 1D) and spatial relationships on an imaginary map of France (Fig. 1E); (2) a non-imagery control task using abstract words (Fig. 1F), and (3) an audio-visual perception task using the same items as in the imagery tasks (Fig. 1G). In the imagery tasks, participants heard a word indicating a particular imagery domain (e.g., “shape”), followed by 2 words, designating the items the participant is required to imagine (e.g. “beaver”, “fox”). They were instructed to generate and maintain mental images as vivid as possible for each item. Eight seconds after the second items, they heard an attribute word (e.g. “long”). They then pressed one of two buttons accordingly, indicating which of the items is most closely associated with the attribute (e.g. which of the animals they associate with the attribute “long”, see schematics in Fig. 1A). Finally, they reported the overall vividness of their mental imagery in that trial, for items and for the two items imagined together during the “imagining” portion, on a 4-level Likert scale by pressing one of 4 buttons of an MR-compatible button box (Current Designs, Philadelphia, USA), where button 1 indicated “no image at all” and button 4 indicated a “vivid and realistic image”. In the shape imagery task, participants had to decide which item was longer or more round. In the color imagery task, participants had to decide which fruit or vegetable had darker or lighter color. In the letters imagery task, participants had to imagine the shape of French words in lowercase and had to decide which word had ascenders (e.g., t, l, d) or descenders (e.g. j, p, y). In the famous-faces imagery task, participants had to decide which celebrity had a more round or oval face. In the map-of-France imagery task, participants had to decide which city was located to the left or the right to Paris. In the non-imagery abstract-word task, participants had to decide which of two abstract words (e.g., “routine”, convention”) was semantically closer to a third word (e.g. “society”). In the perception task, the same stimuli used for the imagery tasks were presented in an audio-visual format. In the abstract-word and the perception tasks participants rated their confidence on a 4-level Likert scale, instead of rating vividness. The auditory stimulus were voice recordings of the corresponding French names per item. All voice recordings were generated in an online TTS engine (https://texttospeechrobot.com/; fr-FR_ReneeVoice) and digitized at a 44.1 kHz sampling rate. The images shown in the perception task were color photographs of the corresponding items on a gray background. The words in letters perception task were rendered in “Monotype Corsiva” font to be visually closer to hand-written letters.

4. Data acquisition

The brain images are acquired using an ultra-high field 7-Tesla Magnetom scanner (Siemens, Erlangen, Germany) with a 1Tx/32Rx head coil (Nova medical, Wilmington, USA) at the NeuroSpin center of the French Alternative Energies and Atomic Energy Commission (CEA). No dielectric pads were used due to the limited space within the head coil with the headphone (OptoActive II, Optoacoustics, Israel). To minimize light reflections inside the head coil, a piece of black paper was inserted to cover the inner surface of the transmitter coil element. Stimuli were presented via a BOLDscreen 32 LCD screen (Cambridge Research Systems, UK, 69.84 x 39.29 cm, resolution=1920 x 1080 pixels, refresh rate=120 Hz, viewing distance ~200 cm), at the head-end of the scanner bore. Participants viewed the screen through a mirror attached to the head coil.

The fMRI scan session lasted 150 minutes in total, split into 5 runs. The first 3 runs consisted of 90 imagery-only trials (30 trials per run, each including 6 trials per domain, 12 min 14 s per run, 367 volumes). The absence of visual perceptual trials prevented potential spillovers of perceptual responses to imagery trials. The last 2 runs consisted of 36 trials each (6 abstract word trials, 15 imagery trials and 15 audio-visual perception trials per run, each including 3 trials per domain, 14 min 38 s per run, 439 volumes), in that order. Notably, items in the imagery trials and perceptual trials of the last two runs are identical. The inter-trial intervals were jittered between 3s and 7s. Importantly, the order of trials within each task type was fully randomized across domains. For each imagery domain, the order of items was counterbalanced, i.e., each item is presented once as the first item and once as the second item. Participants were instructed to keep their eyes open during scans. During the imagery and abstract word tasks, they saw an empty gray screen without fixation cross. During the perception tasks, they saw visual stimuli while simultaneously hearing the corresponding auditory stimuli. The perception tasks also enabled the localization of domain-preferring regions.

Functional data were acquired with a 2D gradient-echo EPI sequence (TR = 2000 ms, TE = 28 ms, voxel size = 1.2 mm isotropic, multiband acceleration factor=2; encoding direction: anterior to posterior, iPAT=3, flip angle = 75, partial Fourier=6/8, bandwidth=1488 Hz/Px, echo spacing=0.78 ms, number of slices=70, no gap, reference scan mode: GRE, MB LeakBlock kernel: off, fat suppression enabled). To correct for EPI distortion, a 5-volume functional run with the opposite phase encoding direction (posterior to anterior) was acquired immediately before each task run. Participants were instructed not to move between these pairs of two runs. Manual interactive shimming of the B0 field was performed for all participants. The

system voltage was set to 250 V for all sessions, and the fat suppression was decreased per run to ensure the specific absorption rate for all functional runs did not surpass 62%. To minimize artifacts and increase signal-to-noise ratio around the ventral temporal cortex, the functional data acquisition slab was tilted in a way that excluded the eyes and the ear canal signal dropout region, so that the ventral temporal cortex especially the anterior occipital-temporal sulcus above the ear canal was covered. However, part of the anterior temporal lobe was not able to be included (Fig.S2A).

High-resolution MP2RAGE anatomical images were obtained between the third and the fourth functional runs (resolution=0.65 mm isotropic, TR=5000 ms, TE=2.51 ms, TI1/TI2=900/2750 ms, flip angles=5/3, iPAT=2, bandwidth=250 Hz/Px, echo spacing=7 ms).

5. Behavioral data analysis

Our behavioral data analysis was similar to that of a study using the same tasks with a more extensive cohort of 117 participants (Liu & Bartolomeo, 2023). We conducted two Bayesian repeated measures ANOVAs were conducted within each modality, with the factors of Group (Aphantasia, Typical imagers) and Domain (Shape, Color, Word, Face, Space). The dependent variables for the imagery tasks were accuracy (arcsine-transformed proportions of correct responses); response times (RTs) and trial-by-trial vividness scores (translated to a 0-1 scale and arcsine-transformed), and for the perceptual tasks were accuracy, RTs and trial-by-trial confidence scores (translated to a 0-1 scale and arcsine-transformed). For each participant, we excluded trials with response times (RT) faster than 150 ms or exceeding three SDs from the participant's mean. Statistical tests were performed using JASP 0.16.2 (https://jasp-stats.org/), and used the JASP default priors. A commonly accepted convention is that Bayes factors (BF10 or BFs) between 3 and 10 indicate moderate evidence in favor of the model in the numerator (H1); BFs between 10 and 30 indicate strong evidence; BFs larger than 30 indicate very strong evidence. The inverse of these cut-offs values provides moderate (0.33-0.1), strong (0.1-0.03), or very strong evidence (<0.03) for the model in the denominator (H0), i.e. the null hypothesis.

6. fMRI data Preprocessing

We processed the fMRI data with BrainVoyager (Version 22.0.2.4572, Brain Innovation, Maastricht, The Netherlands, https://www.brainvoyager.com/), MATLAB (version R2018b), and NeuroElf 1.1 toolbox (http://neuroelf.net/) implemented in MATLAB. The functional data underwent EPI distortion correction using the posterior-to-anterior directional functional volumes (COPE plugin in BrainVoyager), where the in-plane voxel displacement map

between the actual task run and the first volume of the preceding distortion correction run (in reversed phase encoding direction) was computed, and applied to the task run. The distortion-corrected data was then corrected for slice scan time (sinc interpolation, slice scanning order read from the slice time table in the DICOM headers), 3D rigid motion correction (trilinear for estimation, sinc for applying the correction, aligned to the first volume within each run), high-pass temporal filtering (GLM with Fourier basis set, number of cycles=3). No spatial smoothing was applied to the data at this stage.

The MP2RAGE anatomical data consisted of four image types: inversion 1, inversion 2, quantitative T1, uniform. To have a similar appearance to the conventional MPRAGE anatomical data, the uniform image was divided by the T1 image (an optional step), and the background noise was masked out by the inversion 2 image. The resulting anatomical image was resampled to 0.6 mm isotropic (framing cube dimension: 384×384×384), and transformed into Talairach space (TAL). For data visualization, the white matter-gray matter boundary was segmented in TAL space, and reconstructed as surface meshes.

For fMRI across-run co-registration, the fourth functional run was co-registered to the anatomical data, then all the other functional runs were manually co-registered to the fourth functional run. The across-run co-registration quality was inspected visually with animations looping through the first volumes across runs in TAL space. After the quality checks, all functional images were then transformed into TAL space.

After alignment across runs, the functional data of the main experiment were then spatially smoothed with 6 mm FWHM for group-level univariate analysis due to the individual anatomical/functional variability. No spatial smoothing was applied in the case of individual analysis. All results in this study were computed in the volume space.

7. Univariate analysis

Two different general linear models (GLMs) were defined with the following main predictors: 1) five domains in imagery-only trials (5 predictors in total) in the first 3 runs; 2) abstract word and five domains in imagery and in perception trails (11 predictors in total) in the last 2 runs. The period of predictors started from the first domain words to the attribute word before rating periods. For all the GLM models above, the time courses were %-transformed, the main predictors were convolved with a two-gamma hemodynamic response function, and the 6 parameters of participant's head motion were z-scored and entered as confounding factors. AR(2) correction was used for correcting serial correlations. The two GLM models

were applied to both no-smoothed fMRI datasets for individual analysis and 6 mm FWHM smoothed fMRI datasets for group-level analysis.

The contrast of all Imagery *versus* Abstract words, all Imagery *versus* all Perception, all Perception *versus* Abstract words and single perceptual domain *versus* other four domains was conducted with trials in run 4-5. The contrast of all Imagery *versus* baseline and single imagery domain *versus* other four domains was conducted with trials in run 1-3.

The group random-effect GLM analysis was performed for each predictor set with smoothed data. Cluster size thresholds for all group-level contrast maps in this study were estimated using Monte-Carlo simulation (alpha level=0.05, numbers of iterations=5000, initial $p<0.005$), with the BrainVoyager plugin Cluster-Level Statistical Threshold Estimator (https://support.brainvoyager.com/brainvoyager/functional-analysis-statistics/46-tresholding-multiple-comparisons-problem/226-plugin-help-cluster-thresholding), masked with the common functional data coverage across 10 participants in each group.

8. Delineating individual functional foveal V1 and pheripheral V1

Due to the substantial functional variability across participants in EVA (Benson et al., 2022),, we mapped the location of the foveal V1 and the pheripheral V1 in each individual based on brain anatomy and functional activation during perception. For peripheral V1, the individual brain was first co-registered to a functional visual atlas visfAtlas (Rosenke et al., 2021) with linear transformation to each individual's brain anatomy through meticulous manual alignment and thorough visual inspection, particularly in the vicinity of the calcarine sulcus. The foveal V1 was manually delimited in the individual brain in the lateral occipital lobe around the retro calcarine sulcus. The activity profiles of both V1 subregions confirmed its activation during perception.

9. Psychophysiological interactions (PPIs) analysis

To investigate task-specific functional connectivity, we conducted PPI analysis with trials in run 4-5. We built each PPI design matrix by 1) generating a task contrast regressor of two conditions, balanced by a regressor of the sum of two conditions, both convolved with the hemodynamic response function (HRF); 2) extracting a demeaned time course from the seed ROI; 3) generating an interaction regressor as an element-by-element product of the HRF-convolved task contrast and seed ROI regressors; 4) adding the 6 parameters of participant’s z-scored head motion as confounding factors. Specifically, to investigate

domain-general connectivity, we grouped all five imagery domains as a single main condition and all five perception domains as another main condition, and included a separate main condition for Abstract words. In each PPI contrast, a task contrast regressor was established, such as the contrast between all Imagery *versus* Abstract words, which was defined by subtracting the main condition for Abstract words from the main condition for Imagery. On domain-specific connectivity, we built the task contrast regressor by subtracting the Abstract words condition from single domain condition, while keeping the other imagery/perceptual domain conditions unchanged. In BrainVoyager, we conducted GLMs using the PPI design matrix for each contrast separately on fMRI datasets that were smoothed with 6 mm FWHM.

10. Task-residual functional connectivity analysis

In order to identify putative direct upstream or downstream areas within the same functional structure of the FIN in the task, we further performed functional connectivity using task residual data that exploits the variance remaining after removing the mean task-related signal from a time series. We smoothed the task data of the run 1-3 at 6 mm FWHM, regressed out the task-related activity by deconvolution analysis (12 stick predictors per stimulus, covering the evolvement of the BOLD shape per trial) and head motion parameters. Using individual FIN as the seed region, we averaged the extracted residual time course across voxels, and correlated it with the residual time courses of all voxels in each run, resulting in one correlation R map per run. The connectivity pattern across the runs was stable for all participants. The R maps were Fisher's Z-transformed, averaged across runs per participant for group-level comparisons. The resulting group-level maps were thresholded at $p<0.005$ for cluster size correction.

11. Representational similarity analysis (RSA)

To assess the group difference in representational information during imagery, we performed RSA analysis within all imagery domain-general regions activated in the contrast of all Imagery *versus* Abstract words, and additionally within V1. We obtained voxel-wise % signal change from TR 4-5 (normalized by the TRs -2 to 0 as the baseline), corresponding to the maximum activation of the first item and with minimal influence from the second item in each trial. For imagery similarity analysis, we obtained brain activity from 90 imagery trials (18 per domain) in run 1-3. For perceptual similarity analysis, we extracted brain activity from 30 perceptual trials (6 per domain) in run 4-5. In imagery-perceptual similarity comparison, we

used brain activity from imagery trials in run 4-5, which had the same items as in perceptual trials. We calculated the correlation between the multivoxel patterns of each pair of stimuli using the Pearson correlation coefficient to generate a representational dissimilarity matrix (RDM).

References

Aitken, F., Menelaou, G., Warrington, O., Koolschijn, R. S., Corbin, N., Callaghan, M. F., & Kok, P. (2020). Prior expectations evoke stimulus-specific activity in the deep layers of the primary visual cortex. *PLOS Biology*, *18*(12), e3001023. https://doi.org/10/grzhbd

Amalric, M., & Dehaene, S. (2016). Origins of the brain networks for advanced mathematics in expert mathematicians. *Proc Natl Acad Sci U S A*, *113*(18), 4909–4917. https://doi.org/10.1073/pnas.1603205113

Bartolomeo, P. (2002). The Relationship Between Visual Perception and Visual Mental Imagery: A Reappraisal of the Neuropsychological Evidence. *Cortex*, *38*(3), 357–378. https://doi.org/10.1016/s0010-9452(08)70665-8

Bartolomeo, P. (2021). Visual agnosia and imagery after Lissauer. *Brain: A Journal of Neurology*, *144*(9), 2557–2559. https://doi.org/10/grrsd6

Bartolomeo, P., Bachoud-Levi, A. C., Chokron, S., & Degos, J.-D. (2002). Visually- and motor-based knowledge of letters: Evidence from a pure alexic patient. *Neuropsychologia*, *40*(8), 1363–1371. https://doi.org/10/fm5k8g

Bartolomeo, P., Bachoud-Lévi, A.-C., De Gelder, B., Denes, G., Barba, G. D., Brugières, P., & Degos, J.-D. (1998). Multiple-domain dissociation between impaired visual perception and preserved mental imagery in a patient with bilateral extrastriate lesions. *Neuropsychologia*, *36*(3), 239–249. https://doi.org/10.1016/S0028-3932(97)00103-6

Bartolomeo, P., Hajhajate, D., Liu, J., & Spagna, A. (2020). Assessing the causal role of early visual areas in visual mental imagery. *Nature Reviews Neuroscience*, *21*(9), 517–517. https://doi.org/10.1038/s41583-020-0348-5

Bartolomeo, P., & Seidel Malkinson, T. (2019). Hemispheric lateralization of attention processes in the human brain. *Current Opinion in Psychology*, *29*, 90–96. https://doi.org/10/ggbr5v

Bartolomeo, P., & Seidel Malkinson, T. (2022). Building models, testing models: Asymmetric

roles of SLF III networks?: Comment on “Left and right temporal-parietal junctions (TPJs) as ‘match/mismatch’ hedonic machines: A unifying account of TPJ function” by Doricchi et al. *Physics of Life Reviews*, *44*, 70–72. https://doi.org/10/grrsd8

Bartolomeo, P., Vuilleumier, P., & Behrmann, M. (2015). The whole is greater than the sum of the parts: Distributed circuits in visual cognition. *Cortex*, *72*, 1–4. https://doi.org/10/grrsc9

Behrmann, M., Winocur, G., & Moscovitch, M. (1992). Dissociation between mental imagery and object recognition in a brain-damaged patient. *Nature*, *359*(6396), Article 6396. https://doi.org/10.1038/359636a0

Benson, N. C., Yoon, J. M. D., Forenzo, D., Engel, S. A., Kay, K. N., & Winawer, J. (2022). Variability of the Surface Area of the V1, V2, and V3 Maps in a Large Sample of Human Observers. *Journal of Neuroscience*, *42*(46), 8629–8646. https://doi.org/10.1523/JNEUROSCI.0690-21.2022

Bergmann, J., Morgan, A. T., & Muckli, L. (2019). Two distinct feedback codes in V1 for ‘real’ and ‘imaginary’ internal experiences. *bioRxiv*. https://doi.org/10.1101/664870

Binder, J. R., Desai, R. H., Graves, W. W., & Conant, L. L. (2009). Where Is the Semantic System? A Critical Review and Meta-Analysis of 120 Functional Neuroimaging Studies. *Cerebral Cortex*, *19*(12), 2767–2796. https://doi.org/10/c2vp52

Blajenkova, O., Kozhevnikov, M., & Motes, M. A. (2006). Object-spatial imagery: A new self-report imagery questionnaire. *Applied Cognitive Psychology*, *20*(2), 239–263. https://doi.org/10.1002/acp.1182

Brang, D., Towle, V. L., Suzuki, S., Hillyard, S. A., Di Tusa, S., Dai, Z., Tao, J., Wu, S., & Grabowecky, M. (2015). Peripheral sounds rapidly activate visual cortex: Evidence from electrocorticography. *Journal of Neurophysiology*, *114*(5), 3023–3028. https://doi.org/10.1152/jn.00728.2015

Cate, A. D., Herron, T. J., Yund, E. W., Stecker, G. C., Rinne, T., Kang, X., Petkov, C. I., Disbrow, E. A., & Woods, D. L. (2009). Auditory Attention Activates Peripheral Visual

Cortex. *PLOS ONE*, *4*(2), e4645. https://doi.org/10.1371/journal.pone.0004645

Cichy, R. M., Heinzle, J., & Haynes, J. D. (2012). Imagery and perception share cortical representations of content and location. *Cereb Cortex*, *22*(2), 372–380. https://doi.org/10.1093/cercor/bhr106

Conway, B. R. (2018). The Organization and Operation of Inferior Temporal Cortex. *Annual Review of Vision Science*, *4*(1), 381–402. https://doi.org/10.1146/annurev-vision-091517-034202

Corbetta, M., Patel, G., & Shulman, G. L. (2008). The Reorienting System of the Human Brain: From Environment to Theory of Mind. *Neuron*, *58*(3), 306–324. https://doi.org/10.1016/j.neuron.2008.04.017

Crick, F., & Koch, C. (1995). Are we aware of neural activity in primary visual cortex? *Nature*, *375*(6527), Article 6527. https://doi.org/10.1038/375121a0

Dance, C. J., Ipser, A., & Simner, J. (2022). The prevalence of aphantasia (imagery weakness) in the general population. *Conscious Cogn*, *97*, 103243. https://doi.org/10.1016/j.concog.2021.103243

Dehaene, S., Changeux, J.-P., Naccache, L., Sackur, J., & Sergent, C. (2006). Conscious, preconscious, and subliminal processing: A testable taxonomy. *Trends in Cognitive Sciences*, *10*(5), 204–211. https://doi.org/10.1016/j.tics.2006.03.007

Dehaene, S., & Cohen, L. (2011). The unique role of the visual word form area in reading. *Trends in Cognitive Sciences*, *15*(6), 254–262.

D'Esposito, M., Detre, J. A., Aguirre, G. K., Stallcup, M., Alsop, D. C., Tippet, L. J., & Farah, M. J. (1997). A functional MRI study of mental image generation. *Neuropsychologia*, *35*(5), 725–730. https://doi.org/10.1016/S0028-3932(96)00121-2

Dijkstra, N., Bosch, S. E., & van Gerven, M. A. J. (2019). Shared Neural Mechanisms of Visual Perception and Imagery. *Trends in Cognitive Sciences*, *23*(5), 423–434. https://doi.org/10.1016/j.tics.2019.02.004

Epstein, R., Harris, A., Stanley, D., & Kanswisher, N. (1999). The parahippocampal place

area: Recognition, navigation, or encoding? *Neuron*, *23*(1), 115–125. https://doi.org/10/b7jhz8

Farah, M. J. (1984). The neurological basis of mental imagery: A componential analysis. *Cognition*, *18*(1), 245–272. https://doi.org/10.1016/0010-0277(84)90026-X

Fernandino, L., Tong, J.-Q., Conant, L. L., Humphries, C. J., & Binder, J. R. (2022). Decoding the information structure underlying the neural representation of concepts. *Proceedings of the National Academy of Sciences*, *119*(6), e2108091119. https://doi.org/10/gpgvhw

Gaillard, R., Naccache, L., Pinel, P., Clémenceau, S., Volle, E., Hasboun, D., Dupont, S., Baulac, M., Dehaene, S., Adam, C., & Cohen, L. (2006). Direct Intracranial, fMRI, and Lesion Evidence for the Causal Role of Left Inferotemporal Cortex in Reading. *Neuron*, *50*(2), 191–204. https://doi.org/10.1016/j.neuron.2006.03.031

Goldenberg, G. (1993). The neural basis of mental imagery. *Baillieres Clin Neurol*, *2*(2), 265–286.

Grill-Spector, K., & Weiner, K. S. (2014). The functional architecture of the ventral temporal cortex and its role in categorization. *Nature Reviews Neuroscience*, *15*(8), Article 8. https://doi.org/10.1038/nrn3747

Hajhajate, D., Kaufmann, B. C., Liu, J., Siuda-Krzywicka, K., & Bartolomeo, P. (2022). The connectional anatomy of visual mental imagery: Evidence from a patient with left occipito-temporal damage. *Brain Structure and Function*. https://doi.org/10.1007/s00429-022-02505-x

Ishai, A., Ungerleider, L. G., & Haxby, J. V. (2000). Distributed neural systems for the generation of visual images. *Neuron*, *28*(3), 979–990. https://doi.org/10.1016/s0896-6273(00)00168-9

Jackson, R. L. (2021). The neural correlates of semantic control revisited. *NeuroImage*, *224*, 117444. https://doi.org/10.1016/j.neuroimage.2020.117444

Kanwisher, N., McDermott, J., & Chun, M. M. (1997). The Fusiform Face Area: A Module in

Human Extrastriate Cortex Specialized for Face Perception. *Journal of Neuroscience*, *17*(11), 4302–4311. https://doi.org/10.1523/JNEUROSCI.17-11-04302.1997

Kosslyn, S. M., Ganis, G., & Thompson, W. L. (2001). Neural foundations of imagery. *Nat Rev Neurosci*, *2*(9), 635–642. https://doi.org/10/cfmcjh

Kosslyn, S. M., Thompson, W. L., Kim, I. J., & Alpert, N. M. (1995). Topographical representations of mental images in primary visual cortex. *Nature*, *378*, 496–498. https://doi.org/10/cv9rv7

Kourtzi, Z., & Kanwisher, N. (2001). Representation of Perceived Object Shape by the Human Lateral Occipital Complex. *Science*, *293*(5534), 1506–1509. https://doi.org/10.1126/science.1061133

Kriegeskorte, N. (2008). Representational similarity analysis – connecting the branches of systems neuroscience. *Frontiers in Systems Neuroscience*. https://doi.org/10/fh5dft

Lafer-Sousa, R., Conway, B. R., & Kanwisher, N. G. (2016). Color-Biased Regions of the Ventral Visual Pathway Lie between Face- and Place-Selective Regions in Humans, as in Macaques. *Journal of Neuroscience*, *36*(5), 1682–1697. https://doi.org/10.1523/JNEUROSCI.3164-15.2016

Lau, H. C., & Passingham, R. E. (2006). Relative blindsight in normal observers and the neural correlate of visual consciousness. *Proceedings of the National Academy of Sciences*, *103*(49), 18763–18768. https://doi.org/10.1073/pnas.0607716103

Liu, J., & Bartolomeo, P. (2023). Probing the unimaginable: The impact of aphantasia on distinct domains of visual mental imagery and visual perception. *Cortex*, *166*, 338–347. https://doi.org/10.1016/j.cortex.2023.06.003

Liu, J., Bayle, D. J., Spagna, A., Sitt, J. D., Bourgeois, A., Lehongre, K., Fernandez-Vidal, S., Adam, C., Lambrecq, V., Navarro, V., Seidel Malkinson, T., & Bartolomeo, P. (2023). Fronto-parietal networks shape human conscious report through attention gain and reorienting. *Communications Biology*, *6*(730), Article 1.

https://doi.org/10.1038/s42003-023-05108-2

Liu, J., Spagna, A., & Bartolomeo, P. (2022). Hemispheric asymmetries in visual mental imagery. *Brain Structure and Function*, *227*(2), 697–708. https://doi.org/10.1007/s00429-021-02277-w

Mahon, B. Z., & Caramazza, A. (2011). What drives the organization of object knowledge in the brain? *Trends in Cognitive Sciences*, *15*(3), 97–103. https://doi.org/10.1016/j.tics.2011.01.004

Mashour, G. A., Roelfsema, P., Changeux, J.-P., & Dehaene, S. (2020). Conscious Processing and the Global Neuronal Workspace Hypothesis. *Neuron*, *105*(5), 776–798. https://doi.org/10.1016/j.neuron.2020.01.026

Mechelli, A., Price, C. J., Friston, K. J., & Ishai, A. (2004). Where bottom-up meets top-down: Neuronal interactions during perception and imagery. *Cereb Cortex*, *14*(11), 1256–1265. https://doi.org/10.1093/cercor/bhh087

Milton, F., Fulford, J., Dance, C., Gaddum, J., Heuerman-Williamson, B., Jones, K., Knight, K. F., MacKisack, M., Winlove, C., & Zeman, A. (2021). Behavioral and Neural Signatures of Visual Imagery Vividness Extremes: Aphantasia versus Hyperphantasia. *Cerebral Cortex Communications*, *2*(2), tgab035. https://doi.org/10.1093/texcom/tgab035

Morales, J., Lau, H., & Fleming, S. M. (2018). Domain-General and Domain-Specific Patterns of Activity Supporting Metacognition in Human Prefrontal Cortex. *The Journal of Neuroscience*, *38*(14), 3534–3546. https://doi.org/10.1523/JNEUROSCI.2360-17.2018

Moro, V., Berlucchi, G., Lerch, J., Tomaiuolo, F., & Aglioti, S. M. (2008). Selective deficit of mental visual imagery with intact primary visual cortex and visual perception. *Cortex*, *44*(2), 109–118. https://doi.org/10.1016/j.cortex.2006.06.004

O'Craven, K. M., & Kanwisher, N. (2000). Mental imagery of faces and places activates corresponding stiimulus-specific brain regions. *J Cogn Neurosci*, *12*(6), 1013–1023.

https://doi.org/10.1162/08989290051137549

Pearson, J. (2019). The human imagination: The cognitive neuroscience of visual mental imagery. *Nature Reviews Neuroscience*, *20*(10), Article 10. https://doi.org/10.1038/s41583-019-0202-9

Pearson, J., Naselaris, T., Holmes, E. A., & Kosslyn, S. M. (2015). Mental Imagery: Functional Mechanisms and Clinical Applications. *Trends Cogn Sci*, *19*(10), 590–602. https://doi.org/10.1016/j.tics.2015.08.003

Raichle, M. E. (2015). The Brain's Default Mode Network. *Annual Review of Neuroscience*, *38*(1), 433–447. https://doi.org/10.1146/annurev-neuro-071013-014030

Reddy, L., Tsuchiya, N., & Serre, T. (2010). Reading the mind's eye: Decoding category information during mental imagery. *Neuroimage*, *50*(2), 818–825. https://doi.org/10.1016/j.neuroimage.2009.11.084

Rosenke, M., van Hoof, R., van den Hurk, J., Grill-Spector, K., & Goebel, R. (2021). A Probabilistic Functional Atlas of Human Occipito-Temporal Visual Cortex. *Cerebral Cortex*, *31*(1), 603–619. https://doi.org/10.1093/cercor/bhaa246

Santarpia, A., Blanchet, A., Poinsot, R., Lambert, J. F., Mininni, G., & Thizon-Vidal, S. (2008). Évaluer la vivacité des images mentales dans différentes populations françaises. *Pratiques Psychologiques*, *14*(3), 421–441. https://doi.org/10.1016/j.prps.2007.11.001

Shulman, G. L., Astafiev, S. V., McAvoy, M. P., d'Avossa, G., & Corbetta, M. (2007). Right TPJ deactivation during visual search: Functional significance and support for a filter hypothesis. *Cerebral Cortex*, *17*(11), 2625–2633. https://doi.org/10/fhgdwq

Sokolowski, H. M., & Levine, B. (2023). Common neural substrates of diverse neurodevelopmental disorders. *Brain*, *146*(2), 438–447. https://doi.org/10.1093/brain/awac387

Spagna, A. (2022). Chapter 8 - Visual mental imagery: Inside the mind's eyes. In G. Miceli, P. Bartolomeo, & V. Navarro (Eds.), *Handbook of Clinical Neurology* (Vol. 187, pp. 145–160). Elsevier. https://doi.org/10.1016/B978-0-12-823493-8.00010-9

Spagna, A., Hajhajate, D., Liu, J., & Bartolomeo, P. (2021). Visual mental imagery engages the left fusiform gyrus, but not the early visual cortex: A meta-analysis of neuroimaging evidence. *Neuroscience & Biobehavioral Reviews*, *122*, 201–217. https://doi.org/10.1016/j.neubiorev.2020.12.029

Sporns, O., & Betzel, R. F. (2016). Modular Brain Networks. *Annual Review of Psychology*, *67*(1), 613–640. https://doi.org/10.1146/annurev-psych-122414-033634

Stokes, M., Thompson, R., Cusack, R., & Duncan, J. (2009). Top-down activation of shape-specific population codes in visual cortex during mental imagery. *Journal of Neuroscience*, *29*(5), 1565–1572. https://doi.org/10.1523/JNEUROSCI.4657-08.2009

van Vugt, B., Dagnino, B., Vartak, D., Safaai, H., Panzeri, S., Dehaene, S., & Roelfsema, P. R. (2018). The threshold for conscious report: Signal loss and response bias in visual and frontal cortex. *Science*, *360*(6388), 537–542. https://doi.org/10/gc8jfv

Yomogida, Y., Sugiura, M., Watanabe, J., Akitsuki, Y., Sassa, Y., Sato, T., Matsue, Y., & Kawashima, R. (2004). Mental Visual Synthesis is Originated in the Fronto-temporal Network of the Left Hemisphere. *Cerebral Cortex*, *14*(12), 1376–1383. https://doi.org/10.1093/cercor/bhh098

Zeman, A., Dewar, M., & Della Sala, S. (2015). Lives without imagery – Congenital aphantasia. *Cortex*, *73*, 378–380. https://doi.org/10.1016/j.cortex.2015.05.019